PAPER

Spin-polarized tunneling and polaronic transport properties of polycrystalline $(Sm_{1-y}Gd_y)_{0.55}Sr_{0.45}MnO_3$ ($y = 0.5$ and 0.7) compounds

View the article online for updates and enhancements.

IOP ebooks™

Bringing together innovative digital publishing with leading authors from the global scientific community.

Start exploring the collection−download the first chapter of every title for free.

Spin-polarized tunneling and polaronic transport properties of polycrystalline (Sm$_{1-y}$Gd$_y$)$_{0.55}$Sr$_{0.45}$MnO$_3$ ($y = 0.5$ and 0.7) compounds

Dipak Mazumdar[1] , Kalipada Das[2,∗] and I Das[1]

[1] CMP Division, Saha Institute of Nuclear Physics, HBNI, 1/AF, Bidhannagar, Kolkata 700064, India
[2] Department of Physics, Seth Anandram Jaipuria College, 10, Raja Naba Krishna Street, Kolkata 700005, India

E-mail: dmazumdar2306@gmail.com and kalipadadasphysics@gmail.com

Abstract

The detail investigations on the magneto-transport properties of the polycrystalline (Sm$_{0.3}$Gd$_{0.7}$)$_{0.55}$Sr$_{0.45}$MnO$_3$ (SGSMO-1) and (Sm$_{0.5}$Gd$_{0.5}$)$_{0.55}$Sr$_{0.45}$MnO$_3$ (SGSMO-2) compounds, having a glassy-like and ferromagnetic ground states respectively have been carried out in details. Due to the existence of two different magnetic ground states in the above mentioned systems, the magneto-transport properties are markedly differed from each other, specially at the low temperature region. The highly semi-conducting nature of the SGSMO-1 compound is suppressed with the application of magnetic field, whereas the SGSMO-2 compound exhibits a metal–insulator transition in its pristine state. The high-temperature semiconducting state of both the systems can be well-explained with the polaronic transport mechanisms via small-polaron hopping and variable-range-hopping models. The low-temperature metallic states for both the systems are explored by considering the various contributions arise from the grain boundary effect, electron–electron, electron–phonon, electron-magnon etc scattering processes. The spin-polarized tunneling transport mechanism at the grain boundaries plays a crucial role in the enhancement of low-field magnetoresistance in the studied systems.

Keywords: meta-magnetic transition, spin-polarized tunneling, polaron hopping mechanism, glassy-magnetic ground state, ferromagnetic ground state, magnetoresistance

(Some figures may appear in colour only in the online journal)

1. Introduction

In the strongly correlated electronic systems, the coupling between magnetic and magneto-transport properties are extensively studied in the previous few decades [1–8]. The doped perovskite manganite compounds (having the general formula R$_{1-x}$B$_x$MnO$_3$, R = rare earth trivalent ion and B = alkaline earth bivalent ion) are one of the most well-studied systems due to the existence of a strong correlation in between various degrees of freedom like charge, spin, orbital and lattice. The introduction of Mn^{4+} ions in the doped perovskite manganite compounds leads many charming and tunable physical properties compared to its undoped counterpart [9–14]. The tunability of several magnetic (or electrical) ground states by optimizing the dopant elements and concentration (x) also intensify this field from fundamental as well as technological perspectives [7, 13–17]. It is well-established that generally charge-ordered antiferromagnetic (CO-AFM) and ferromag-

netic (FM) doped perovskite manganite compounds possess insulating and metallic ground states respectively below the respected transition temperatures, suggesting the strong correlation between magnetism and electronic properties. However, the scenario becomes quite different in case of the disordered FM or glassy systems having short-range-type of interactions [18–20]. Moreover, the distinguished nature of the physical properties can also be observed in presence of the external magnetic field. Regarding the context of doped manganite materials, it is worth mentioning that metal–insulator transition (MIT) is one of the most observed generic feature. The MIT occurs due to the competing nature of various magnetic phases i.e. coexistence of magnetic phases take place in the system. Since, the phase coexistence drastically changes with magnetic field, the MIT is also influenced by the strength of the external magnetic field. With increasing the field value, MIT temperature (T_{MI}) gradually shifts to the higher temperature side [21]. For a system obeying a continuous FM to paramagnetic (PM) phase transition without any thermal hysteresis, the MIT takes place in a large temperature scale and it will be reversible in nature [21]. The scenario will be completely different for the systems having frustrated or glassy-like magnetic ground state. Here, the resistivity drops drastically within a short span of temperature and a well-pronounced thermal hysteresis has been noticed in those systems [21].

Due to the existence of several fascinating physical properties with the various values of 'x', both $Sm_{1-x}Sr_xMnO_3$ and $Gd_{1-x}Sr_xMnO_3$ compounds are very much studied among the manganite families [20, 22–28]. $Sm_{1-x}Sr_xMnO_3$ possesses both CO-AFM-insulating state and FM metallic (FMM) state depending upon the operating temperature scale [22–26]. In case of half-doped $Gd_{1-x}Sr_xMnO_3$ ($x = 0.5$) compound, a cluster-glass phase is coexisted along with the charge-ordered state at the low temperature regions [27]. Continuing from the discussion about $Sm_{1-x}Sr_xMnO_3$ and $Gd_{1-x}Sr_xMnO_3$ compounds, if we keep the Sr-content fixed ($x = 0.45$) and then double doping of rare-earth site with different compositions like $(Sm_{0.3}Gd_{0.7})_{0.55}$ and $(Sm_{0.5}Gd_{0.5})_{0.55}$, the as-formed compounds exhibited two distinct magnetic ground states such as charge-ordered glassy magnetic state and FMM state respectively [19, 29]. Considering these facts, as $y = 0.5$ and 0.7 compounds lie in both sides of the crossover boundary i.e. $y = 0.6$, we have selected $(Sm_{0.3}Gd_{0.7})_{0.55}Sr_{0.45}MnO_3$ (SGSMO-1) and $(Sm_{0.5}Gd_{0.5})_{0.55}Sr_{0.45}MnO_3$ (SGSMO-2) compounds with two different magnetic ground states for the present study. We have already studied the magnetic and magnetocaloric properties of the SGSMO-1 and SGSMO-2 compounds [19]. According to our earlier report, the value of magnetic entropy change enhanced in the lower Gd-based SGSMO-2 compound as compared to the higher Gd-based SGSMO-1 compound. Additionally, the variation of magnetic cooling capacities (both relative cooling power and refrigerant capacity) exhibited two distinct features [19]. Such anomalies in magnetic and magnetocaloric properties were addressed considering different magnetic configurations of the compounds. To fulfill the criteria of a suitable magnetic refrigerant material, the material should be tested from the view point of the electronic ground state.

The insulating nature of a material is considered as a beneficial parameter for the selection of a magnetic refrigerant material [30].

The motivation of the present work is to explore the influence of different competing magnetic as well as electronic ground states in the electrical and magneto-transport properties of the SGSMO-1 and SGSMO-2 compounds. Additionally we have extended our study even in the PM region. Our study reveals that the electron localization length, electron density at the Fermi level, activation energies are drastically modified depending upon the nature of the magnetic ground state as well as strength of the applied magnetic field.

2. Experimental details

The conventional solid-state reaction mechanism had been employed to prepare the polycrystalline $(Sm_{1-y}Gd_y)_{0.55}Sr_{0.45}MnO_3$ ($Y = 0.5$ and 0.7) (SGSMO) compounds [19]. The x-ray diffraction (XRD) study of the powdered SGSMO-1 and SGSMO-2 confirmed the single-phase nature of the compounds. The profile fitting of the XRD pattern revealed that both the compounds exhibited orthorhombic unit cell with *Pbnm* space group [19]. Both the zero-field and magnetic field dependent electrical resistivity measurements were performed in rectangular bar-shaped samples by four probe method using longitudinal geometry inside a variable temperature cryostat (Cryogenic, UK).

3. Results and discussions

3.1. Evolution of temperature and magnetic field dependence of electrical resistivity

The temperature-dependent of electrical resistivity for both the compounds SGSMO-1 and SGSMO-2 in absence as well as in presence of the external magnetic fields have been displayed in figures 1(a) and (b) respectively. The resistivity data were recorded during cooling and warming cycles. The temperature-dependent resistivity data indicates the semiconducting (insulating) nature of the compounds with decreasing the temperature. For the SGSMO-2 sample, the signature of charge ordering is found at $T \sim 170$ K. However, it is hindered in case of the SGSMO-1 compound. With further lowering the temperature especially below 100 K, an insulator to metal transition has been appeared in the SGSMO-2 compound even in the absence of any external magnetic field. In contrast to that, resistivity of SGSMO-1 sample indicates insulating nature in the whole measured temperature span for $H = 0$ kOe. For the SGSMO-1 compound, the increasing nature of the resistivity may be associated with the glassy magnetic ground state present in the low temperature region [19, 31, 32]. However, with the application of external magnetic field ($H \geqslant 10$ kOe), a well-pronounced MIT is observed in this compound. Such MIT in doped perovskite manganites generally addresses by considering the spontaneously phase transformation from insulating to metallic region with lowering the temperature in the presence of different external magnetic fields [8, 31]. In both the samples, the thermal
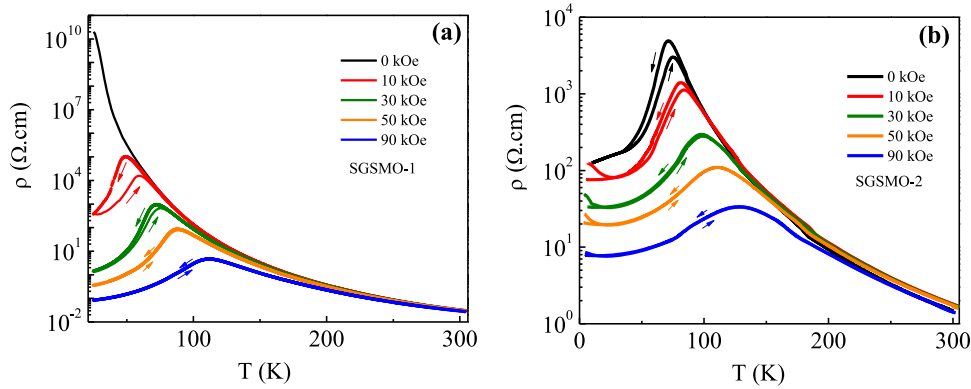
Figure 1. Temperature dependence of electrical resistivity (ρ) in absence of magnetic field as well as in presence of various external magnetic fields for (a) SGSMO-1 and (b) SGSMO-2 compounds respectively. The arrows are used to indicate the direction of the warming and cooling cycles.
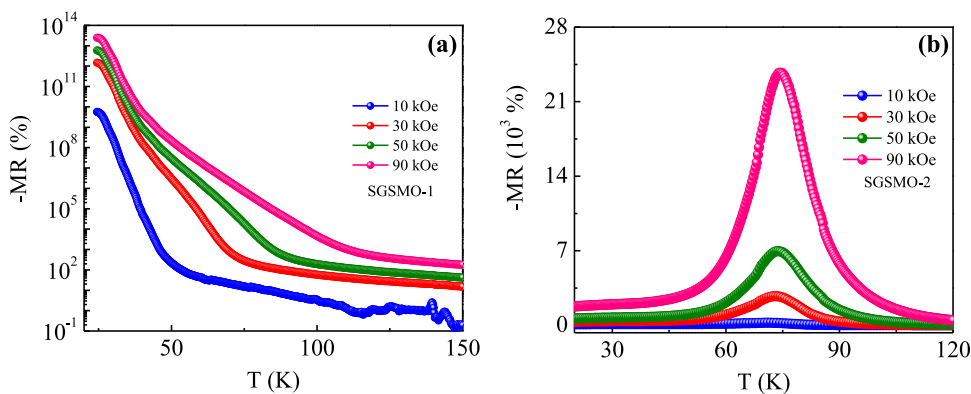

Figure 2. Variation of magnetoresistance (MR) with temperature for different field values for (a) SGSMO-1 and (b) SGSMO-2 compounds respectively.

hysteresis between cooling and warming cycles are reduced with increasing the strength of magnetic fields.

From the temperature-dependent of the electrical resistivity data, we have calculated the magnetoresistance (MR) by using the mathematical expression as given below that is mostly used for the CMR materials [1, 2],

$$\mathrm{MR}\% = \frac{R(H) - R(0)}{R(H)} \times 100\%. \tag{1}$$

Variation of the MR with temperature at different external magnetic field values for both the SGSMO-1 and SGSMO-2 compounds are presented in figures 2(a) and (b) respectively. With decreasing the temperature, a non-saturating tendency is observed in the SGSMO-1 compound and finally it reaches the measurement instrumentation limit at the low temperature region ($T < 25$ K). On the other hand, MR(T) of the SGSMO-2 sample exhibits maximum value at the vicinity of the MIT region.

To get a better view about the modification of magnetic ground state configuration, we have carried out the field-dependent resistivity measurements at some selected temperatures as depicted in the figure 3. Our experimental results indicate that, in case of SGSMO-1 sample with glassy magnetic ground state, a sharp field-induced meta-magnetic type

transition (from insulating to metallic) has been taken place. In contrast to that, for the SGSMO-2 sample having a FM ground state, the resistivity decreases with increasing the strength of the magnetic fields and gradually ground state of the sample converts into a low-resistive metallic state. Such nature may be observed due to the presence of sufficient percolation paths in the SGSMO-2 compound. Moreover, the resistivity should also be less for ordered magnetic state due to the less scattering of conduction electrons. In the presence of magnetic field, the AFM insulating counterpart transformed into the metallic part. After the subsequent field cycling at the specified temperatures, the compound exhibits low resistive metallic state. For the clarity, the magnetic field variation of the four-quadrant resistivity, except the virgin state of the SGSMO-2 sample at $T = 3$ K, is presented in the inset of figure 3(b).

Magnetic field-dependent of MR for both the compounds were also calculated by using the conservative definition [1, 2] used for various metallic systems is given below

$$\mathrm{MR}\% = \frac{R(H) - R(0)}{R(0)} \times 100\%. \tag{2}$$

From the fundamental point of view, it is beneficial to extract the low-field MR values. In this present study, a sharp
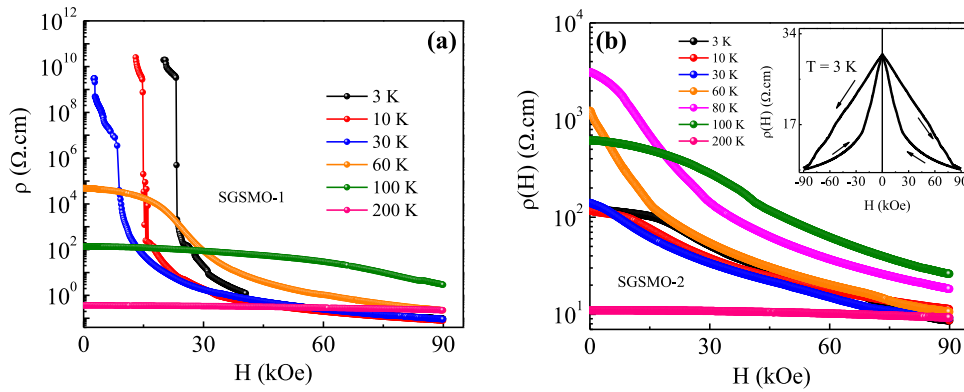
Figure 3. Evolution of electrical resistivity at different constant temperatures with magnetic field sweeping over 0 kOe to 90 kOe under the zero-field cooled condition i.e. the virgin curves for (a) SGSMO-1 and (b) SGSMO-2 compounds respectively. Inset of (b) shows the four-quadrant variation of resistivity except the virgin curve with magnetic field recorded at $T = 3$ K for SGSMO-2 compound. The arrows are used to show the direction of the field-sweeping.
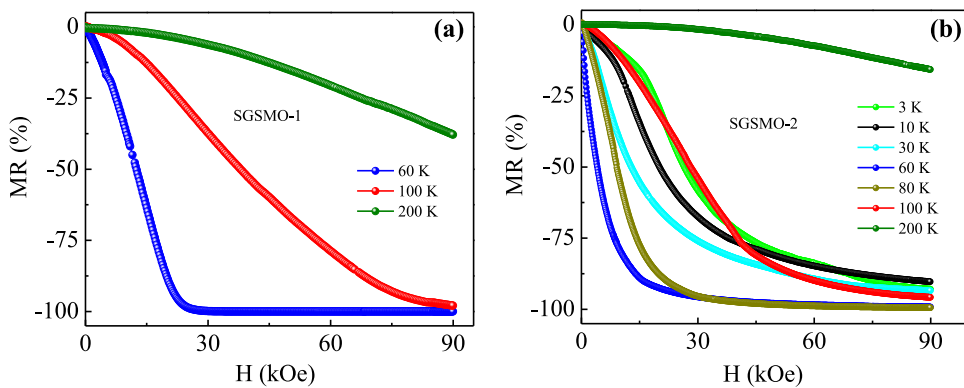

Figure 4. Magnetoresistance (MR) as a function of magnetic field calculated for various constant temperatures for (a) SGSMO-1 and (b) SGSMO-2 compounds respectively.

jump in the resistivity from the insulating ground state to a metallic state is observed at the low-temperature region for the SGSMO-1 sample. However, such a sharp meta-magnetic transition vanishes at the high temperature ($T > 10$ K) region. In case of the FM SGSMO-2 compound, due to the increment of external magnetic field, magnetic randomness of the sample decreases. Since resistivity is directly related with the magnetic randomness, it is also be reduced and hence MR should be increased with increasing the field values. In this scenario, the magnetic field-induced sharp meta-magnetic transition is absent. Although, a sharper drop in the low-field ($H < 30$ kOe) MR is present in the SGSMO-2 compound. The easy alignment of the FM domains in the SGSMO-2 compound (compared to the SGSMO-1 compound) may have the significant contribution in enhancement of the low field MR (figure 4).

It is well-documented that for the FM granular system, the low-field MR phenomenon is generally governed by the spin polarized tunneling (SPT) transport mechanism through the grain boundaries [33–35].

3.1.1. Spin-polarized tunneling transport. To understand the basic mechanism behind the magnetic field-dependent of MR in case of our systems, we have utilized the

phenomenological model proposed by Raychaudhuri *et al* by considering the fact of progressive movement of the domain walls across the polycrystalline grain boundaries pinning centers under the application of magnetic field [33, 34]. According to this model, the total MR can be expressed in the following form,

$$\text{MR} = -A' \int_0^H f(k) \mathrm{d}k - JH - KH^3. \tag{3}$$

The first term in the above equation is the contribution arises from the SPT part, which help to drop the resistance sharply at the low-field values and the rest of the two terms arise due to the intrinsic contribution (INT), originating from the double exchange interaction between the two neighboring Mn-cations. Here, J and K are some adjustable fitting parameters [33, 35, 36].

Within this model, it is assumed that the FM domain boundaries are strongly pinned at the pinning centers of the grain boundary with a pinning strength, k in absence of any magnetic field [33, 35]. This pinning strength, k follows a Gaussian-type distribution function $f(k)$ which can be written as

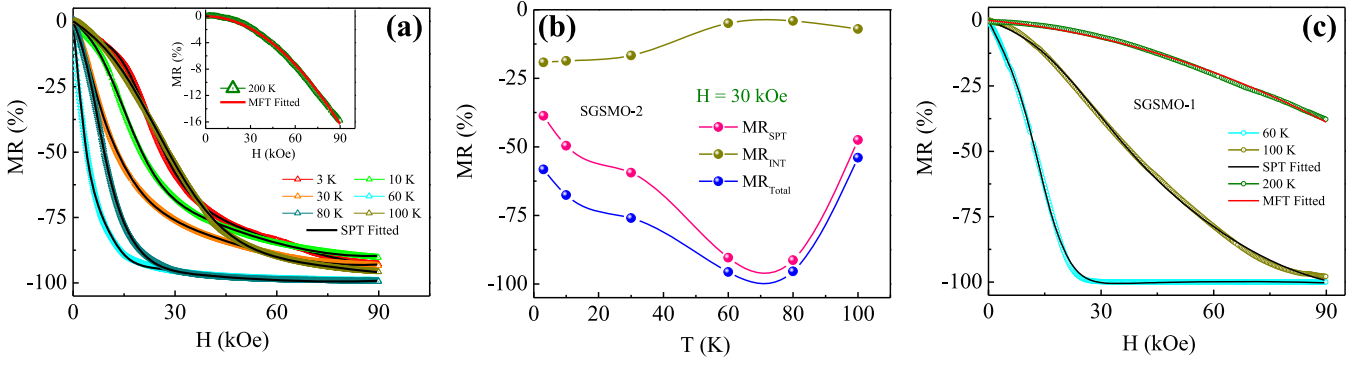$$f(k) = A \exp(-Bk^2) + Ck^2 \exp(-Dk^2), \tag{4}$$

Figure 5. (a) Main panel shows the variation of well-fitted MR with magnetic field by the SPT model at some selected temperatures for the SGSMO-2 compound. The black lines are the best fitting of the MR data using equation (3). The inset shows a typical fitting of MR vs *H* data with the MFT model at $T = 200$ K. The red line represents the best fitting of the experimental data points with the MFT model; (b) temperature dependent of SPT component (MR_{SPT}), intrinsic component (MR_{INT}) and the overall MR (MR_{Total}) extracted for $H = 30$ kOe from the adjustable fitting parameters of the fitted lines as shown in the main panel of figure (a); (c) plot of MR vs *H* for SGSMO-1 compound and its fitting with two different models SPT ($T = 60$ K and 100 K) and MFT ($T = 200$ K), where black and red solid lines are the fitted lines for SPT model and MFT model respectively.

where *A*, *B*, *C*, and *D* are some adjustable fitting parameters used to calculate the SPT contribution to the MR (MR_{SPT}) and the intrinsic contribution to the MR (MR_{INT}) which are given by

$$MR_{SPT} = -A^{/} \int_0^H f(k) \mathrm{d}k \qquad (5)$$

and

$$MR_{INT} = -JH - KH^3. \qquad (6)$$

Using the best fitting parameters as mentioned above, we have fitted the field-dependent of MR curves for various temperatures in case of the FM SGSMO-2 system as presented in figure 5(a). The well-pronounced concave nature of the MR curves are well-understood by the SPT transport mechanism. We have extracted the MR_{SPT} and MR_{INT} parts by using the adjustable fitting parameters as mentioned above. Figure 5(b) displays the variation of overall MR (MR_{Total}), MR_{SPT} and MR_{INT} with temperature for an applied magnetic field of $H = 30$ kOe for the SGSMO-2 compound. Both the MR_{Total} and MR_{SPT} follows the same decreasing trend with increasing the temperature. After reaching a minimum value near the T_C of the system, both of the terms tends to increase with further increasing the temperature. However, the intrinsic contribution of the MR, MR_{INT} increases slowly with increasing temperature, expected for the FM double exchange interaction [33–35]. We have also checked the variation of the MR_{SPT} and MR_{INT} individually as a function of magnetic field for any constant temperature, which is not presented herewith. Above a particular magnetic field value, the SPT contribution to the total MR remains same up to the highest measurable field values of 90 kOe.

However, in case of the SGSMO-1 compound, MIT is observed due to the application of magnetic field. At the low temperature region, the system shows an insulating behavior up to a certain magnetic field value as shown in figure 3(a). The sharp field-induced FMM state from any AFM-insulating state at $T = 3$ K and 10 K in the resistivity data could not be fitted by the SPT model. But the continuous variation of resistivity

(or MR) at the low fields and almost saturating MR values at the high field regions can be described by the SPT model. The excellent fitting of the experimental data points with the SPT model for the SGSMO-1 compound is displayed in figure 5(c) for $T = 60$ K and 100 K. The estimated values of the MR_{SPT} follow the same trend with magnetic field as mentioned in case of the SGSMO-2 compound [35, 37].

Surprisingly, the concave nature of MR at low temperature changes into a convex-type at high temperature ($T = 200$ K) for both the SGSMO-1 and SGSMO-2 compounds as shown in figures 3(a) and (b) respectively. It was reported in the literature that the magnetic field dependent of MR follows a power-law dependence of field at the high temperature PM ground state. We have fitted the magnetic field dependent of MR at $T = 200$ K with a power-law derived from mean-field theory (MFT) of the form $MR = AH + BH^2$, where *A* and *B* are constants [1, 2, 38, 39]. The experimentally calculated MR data points at $T = 200$ K are in excellent agreement with the MFT fitted lines as shown in the inset of figure 5(a) and in the main panel of figure 5(c) for the SGSMO-2 and SGSMO-1 compounds respectively. Therefore, our studied systems obey the PM state at this high temperature region according to the magnetic polaron hopping model which states that the negative MR is proportional to the Brillouin function (B_J) in the FM state and B_J^2 in the PM region for doped manganite systems [38–41].

3.2. Polaronic transport mechanism

To understand the transport mechanism in different temperature regimes of the resistivity data in presence and absence of magnetic fields, various well-known theoretical models have been utilized in the respected temperature scale. For this purpose, we have categorized the whole resistivity data in two different sections viz the high-temperature insulating regime ($T > T_{MI}$) and the low-temperature metallic regime ($T < T_{MI}$). Here, we must mention that we have used only warming cycle data for the analysis of the polaronic transport mechanism.
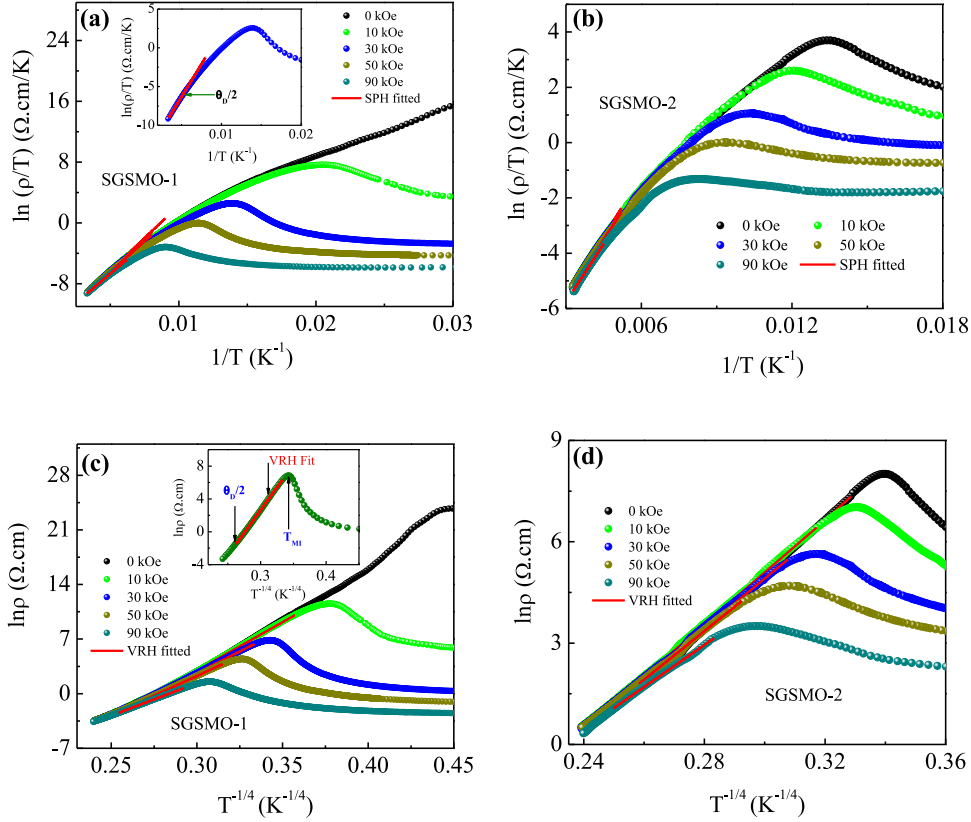
Figure 6. Small polaron hopping (SPH) model: variation of $\ln(\rho/T)$ as a function of inverse temperature ($1/T$) in zero magnetic field as well as in presence of different external magnetic fields for (a) SGSMO-1 and (b) SGSMO-2 compounds respectively. The red straight lines are the best fitting of the experimental data points with the SPH model up to a fixed temperature $\theta_D/2$ (θ_D is the Debye temperature) which is shown in the inset of figure (a). Variable range hopping (VRH) model: the relation between $\ln\rho$ vs $T^{-1/4}$ with and without magnetic field for (c) SGSMO-1 and (d) SGSMO-2 compounds respectively. The red straight lines are used to show the best fitting of experimental data points with VRH model in the limited temperature range of $T_{MI} < T < \theta_D/2$ which is shown in the inset of figure (c) as representative.

3.2.1. High-temperature insulating region. In order to get the clear view of the conduction physics in the studied manganite systems, different models have been employed in order to verify the veracity of the conduction mechanism. In case of the semiconductor and insulator, the band gap model having activation energy, E_A is widely used [28]. The expression of the band gap model in the following form $\rho = \rho_0 \exp(E_A/k_B T)$ must exhibit an Arrhenius temperature dependence plot i.e. a straight line behavior in between $\log \rho$ and $1/T$ must be expected [42, 43]. In our case, we did not observe any such kind of linearity in $\log \rho$ vs $1/T$ plot, suggesting the rejection of the band gap model to describe the conduction mechanism in the present studied systems. Alternatively, one can use two different models viz small polaron hopping (SPH) and variable range hopping (VRH) models in the two different sections of the resistivity data above T_{MI} [44–49]. The SPH model is applicable when the thermal energy is not enough high to overcome the deep potential well where electrons are trapped. In this case, the electron with higher energy is first activated to an intermediate state. The thermal energy received by any second phonon helps to hop out that electron from the intermediate state to its nearest neighbor state easily [28]. According to the SPH model, the expression for the resistivity is given by the relation,

$$\rho = AT \exp(E_P/k_B T), \qquad (7)$$

where $A = k_B/\nu_{ph} Ne^2 R^2 C(1 - C)\exp(2\alpha R)$, E_P is the activation energy for the polaronic hopping process of conduction electrons, k_B is the Boltzmann constant, N is the number of ion sites per unit volume, R is the average inter-site spacing calculated from the relation $R = (1/N)^{1/3}$, C is the fraction of sites occupied by a polaron, α is the electron wave function decay constant and ν_{ph} is the optical phonon frequency having the expression $\nu_{ph} = k_B \theta_D/h$, θ_D is the Debye temperature [44]. The value of $\theta_D/2$ can be estimated from the temperature at which a deviation from the linearity starts in the $\ln(\rho/T)$ vs $1/T$ plot as shown in the inset of figure 6(a) as a representative [44, 45]. The values of as calculated ν_{ph} are in the (8–10) THz range for both the compounds. Although, the SGSMO-2 system possesses higher values of ν_{ph} as compared to the SGSMO-1 compound. The application of the SPH model in the high temperature resistivity data in the temperature above $\theta_D/2$ with and without magnetic fields for the SGSMO-1 and SGSMO-2 compounds have been shown in figures 6(a) and (b) respectively. From the slope of the $\ln(\rho/T)$ vs $1/T$ plot curve, we have estimated the values of E_P for various applied magnetic fields, which are tabulated in table 1 for both the SGSMO-1 and SGSMO-2 compounds. The value of E_P decreases with the increasing magnetic field values supports the delocalization of the conduction e_g electrons. This

Table 1. The calculated parameters obtained from the fitting of the SPH and VRH models in the temperature dependence of resistivity data in the temperature below T_{MI} for both the SGSMO-1 and SGSMO-2 compounds. Here E_P is the polaron activation energy obtained from the slope of the $\ln(\rho/T)$ vs T^{-1} plot; T_0, $N(E_F)$, R_h and W_h are the characteristic temperature, density of states at the Fermi level, most probable hopping distance and hopping energy respectively obtained from the fitting of VRH model (equations (8)–(11)) in the respected ρ vs T data.

	$(Sm_{1-y}Gd_y)_{0.55}Sr_{0.45}MnO_3$ ($y = 0.7$) (SGSMO-1)				
	SPH model	VRH model			
H (kOe)	E_P (meV)	$T_0 \times 10^8$ (K)	$N(E_F) \times 10^{17}$ (eV^{-1}cm^{-3})	R_h (Å) 300 K	W_h (meV) 300 K
0	147.6	2.48	7.92	86.8	195.0
10	146.2	2.39	8.21	85.9	193.1
30	145.3	1.51	13.05	76.5	171.9
50	139.5	1.04	18.77	69.9	157.1
90	132.8	0.48	40.08	57.5	129.3
	$(Sm_{1-y}Gd_y)_{0.55}Sr_{0.45}MnO_3$ ($y = 0.5$) (SGSMO-2)				
	SPH model	VRH model			
H (kOe)	E_P (meV)	$T_0 \times 10^7$ (K)	$N(E_F) \times 10^{18}$ (eV^{-1}cm^{-3})	R_h (Å) 300 K	W_h (meV) 300 K
0	118.4	4.37	4.51	56.1	126.2
10	126.1	3.53	5.59	53.2	119.7
30	123.5	2.90	6.81	50.6	113.9
50	120.4	2.68	7.36	49.6	111.7
90	120.5	1.49	13.25	42.9	96.6

delocalization of electrons facilitates the easy hopping of the electrons to the nearby neighboring states [44, 46, 47]. The estimated values of θ_D as obtained from the $\ln(\rho/T)$ vs $1/T$ plots for both the compounds increase with increasing the strength of magnetic fields. The value of θ_D varies from 400 K to 480 K and 408 K to 512 K for the SGSMO-1 and SGSMO-2 compounds respectively upon application of magnetic fields from 0 kOe to 90 kOe.

We observed that alone the SPH model cannot explain the conduction mechanism below a certain temperature $\theta_D/2$. To explain the conduction process in the low temperature region ($T_{MI} < T < \theta_D/2$, except the zero-field resistivity data of SGSMO-1 compound), the Mott's VRH model is widely used in case of the manganite systems. According to the VRH model, at low temperature region, loosely trapped electrons (large polaron) cannot directly hop to their nearest neighbors due to the lack of sufficient thermal energy [28]. With the phonon assistance, they can easily hop to a small potential difference site [28]. Due to the variation of hopping range for this loosely trapped electrons, it is called VRH. In case of the three dimensional system, the VRH model for resistivity [42, 44, 46] can be expressed as

$$\rho = \rho_0 \exp{(T_0/T)^{1/4}}, \tag{8}$$

where ρ_0 is the residual resistivity and T_0 is the characteristic temperature which can be expressed as

$$T_0 = \frac{24}{\pi N(E_F)k_B\xi^3}. \tag{9}$$

Here $N(E_F)$ is the density of states at the Fermi level and ξ is the localization length [46, 49].

One can also calculate the most probable hopping distance, $R_h(T)$ and the hopping energy, $W_h(T)$ from the T_0 for a given temperature, T by using the following expressions [45, 46]

$$R_h(T) = \frac{3}{8}\xi\left(\frac{T_0}{T}\right)^{1/4} \tag{10}$$

$$W_h(T) = \frac{1}{4}k_B T^{3/4}(T_0)^{1/4}. \tag{11}$$

Figures 6(c) and (d) show the $\ln\rho$ vs $T^{-1/4}$ plots along with the VRH model fitted lines in the respected temperature regime with $H = 0$ kOe and $H \neq 0$ kOe for the SGSMO-1 and SGSMO-2 compounds respectively. Due to the merging of all data points in the high temperature PM region, one cannot clearly visualize the VRH model fitted lines for various magnetic fields. We present a representative VRH model fitting in the temperature range of $\theta_D/2 < T < T_{MI}$ in the inset of figure 6(c). The linear behavior of the VRH model fitted lines help us to estimate the value of T_0 from its slope. Using this values of T_0 in equation (9) for various field values, we have calculated the density of states at the Fermi level ($N(E_F)$) and the values of $N(E_F)$ are presented in table 1 for both the SGSMO-1 and SGSMO-2 compounds respectively. The value of T_0 decreases with increasing magnetic field for both the compounds. With increasing magnetic field, the value of $N(E_F)$ increases due to delocalization of charge carriers and they get sufficient percolation path for the conduction process. By taking the localization length, $\xi = c = $ lattice parameter of the unit cell obtained from the XRD data analysis, we have calculated both R_h and W_h at room temperature ($T = 300$ K) which are also listed in table 1. The decreasing trend of both R_h and W_h with increasing the applied magnetic field values indicates the delocalization of the charge carriers. The as
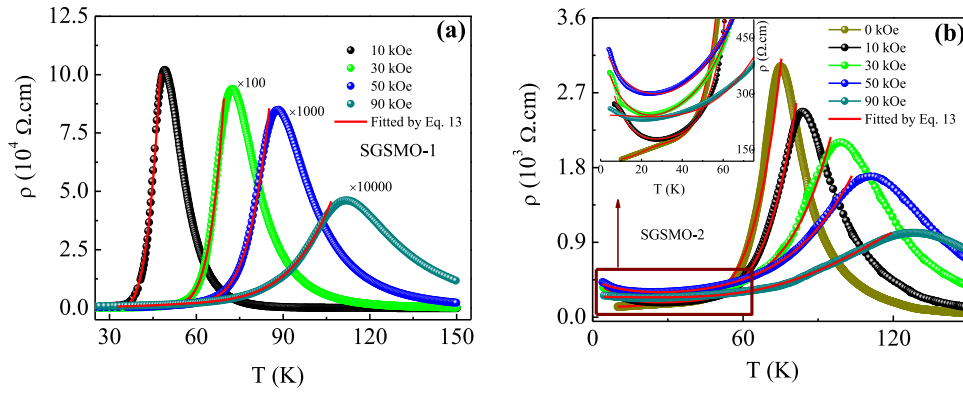
Figure 7. Temperature dependence of electrical resistivity at the low-temperature regime with and without magnetic fields for (a) SGSMO-1 and (b) SGSMO-2 compounds respectively. The red solid lines in these plots represent the best fit of experimental data points in the metallic regime below T_{MI} using equation (13). The inset of figure (b) shows the magnified view of the very low-temperature resistivity data along with the fitted curves for the SGSMO-2 compound.

Table 2. The extracted best fitting parameters from the low-temperature resistivity data using equation (13) in the temperature range below T_{MI} for both the SGSMO-1 and SGSMO-2 compounds. For definition of parameters, see the main text.

		$(Sm_{1-y}Gd_y)_{0.55}Sr_{0.45}MnO_3$ ($y = 0.7$) (SGSMO-1)			
H (kOe)	ρ_0 (Ω cm)	$\rho_{0.5}$ (Ω cm K$^{-0.5}$)	ρ_2 (Ω cm K^{-2})	$\rho_{4.5}$ (Ω cm K$^{-4.5}$)	ρ_5 (Ω cm K^{-5})
10	5.58×10^5	1.76×10^5	7.15×10^2	-1.62×10^{-1}	2.01×10^{-2}
30	3.13×10^4	7.43×10^3	1.27×10^1	-7.32×10^{-4}	6.91×10^{-5}
50	9.45×10^2	2.11×10^2	3.03×10^{-1}	-1.27×10^{-5}	1.13×10^{-6}
90	1.40×10^0	3.37×10^{-1}	6.58×10^{-4}	-3.53×10^{-8}	3.35×10^{-9}
		$(Sm_{1-y}Gd_y)_{0.55}Sr_{0.45}MnO_3$ ($y = 0.5$) (SGSMO-2)			
H (kOe)	ρ_0 (Ω cm)	$\rho_{0.5}$ (Ω cm K$^{-0.5}$)	ρ_2 (Ω cm K^{-2})	$\rho_{4.5}$ (Ω cm K$^{-4.5}$)	ρ_5 (Ω cm K^{-5})
0	173.7	21.2	2.1×10^{-1}	-6.13×10^{-5}	7.86×10^{-6}
10	255.0	48.8	1.3×10^{-1}	-1.82×10^{-5}	2.15×10^{-6}
30	66.1	9.3	2.2×10^{-2}	-1.38×10^{-6}	1.56×10^{-7}
50	32.3	3.3	6.1×10^{-3}	-8.86×10^{-8}	1.26×10^{-8}
90	8.0	0.02	2.4×10^{-4}	-6.65×10^{-8}	4.89×10^{-9}

calculated hopping distance, R_h is found to be higher than the Mn–O–Mn distance and the hopping energy, W_h is also satisfied the condition $W_h \gg k_B T$ for the acceptance of VRH model [48, 50]. These observations are consistent with the earlier reported data in the literature for manganite systems. The value of $N(E_F)$ for SGSMO-1 is one order less than that for SGSMO-2. As pointed out by Jung *et al*, higher values of $N(E_F)$ initiates the adiabatic hopping process [51]. In our case, one order difference in magnitude of $N(E_F)$ may be affected the conduction process for both the compounds. In summary of the above results, we observe that the application of magnetic field decreases the localization length, help to increase the number of delocalized charge carriers which causing the enhancement in the value of $N(E_F)$.

Therefore, the two models viz SPH and VRH have been utilized to understand the conduction mechanism in the temperature dependence of resistivity data above the MIT temperature, T_{MI}.

3.2.2. Low-temperature metallic region. The metallic nature of the resistivity data in the low temperature region below T_{MI} is generally governed by the ferromagnetism in case of the manganite systems. In the present case, we observe a metallic behavior in the ρ vs T plots below T_{MI} in both the SGSMO-1 and SGSMO-2 compounds. The difference in the metallic region between the two compounds is that in SGSMO-1, a MIT takes place due to the application of magnetic field of $H \geqslant 10$ kOe, whereas due to the FM ground state of the SGSMO-2 compound, resistivity decreases with decreasing temperature in absence of any magnetic field. In this case, the conductivity is directed by the FM double exchange interaction of Mn^{3+} and Mn^{4+} ions via O^{2-} ion as proposed by Zener [52]. The variation of the electrical resistivity at the low temperature region ($T < T_{MI}$) can be explained with the help of temperature-dependent polynomial equation, consists with various terms associated with the different scattering mechanisms [44, 46, 53–56]. One of the mostly used polynomial

equation to describe the low-temperature resistivity data is given by the following relation [44, 46, 53]

$$\rho = \rho_0 + \rho_2 T^2 + \rho_{4.5} T^{4.5}. \tag{12}$$

The first term ρ_0 in the above equation is the temperature independent residual resistivity arises due to the defects, grain or domain boundary effects, scattering by impurities etc [44, 46, 49]. Due to the presence of several grain boundaries in the polycrystalline material, ρ_0 plays a vital role in the low-temperature conduction process. The second term $\rho_2 T^2$ arises in the resistivity resulted from the electron–electron scattering phenomenon [49, 54] and the last term $\rho_{4.5} T^{4.5}$ is used to describe the electron-magnon scattering process in the FM region [44, 49, 55].

We tried to fit the resistivity data with the above equation in the low temperature limit, but could not get any satisfactory fitted result. A resistivity minimum has been observed in the low temperature resistivity data of the SGSMO-2 compound. This upturn of resistivity may be explained with the help of Kondo effect which arises due to the scattering from a magnetic impurity in a nonmagnetic lattice [56]. This minima in resistivity should dissolve upon application of magnetic field. However, as seen in figure 7(b), magnetic field does not cause any impact on the resistivity minima, supporting the absence of Kondo-like scattering in the studied system. Due to the strongly correlated nature of the manganite compounds, one has to account the electron–electron (e–e) and electron–phonon (e–ph) interactions. Considering all these facts in the low-temperature resistivity data, two more terms have been included in equation (12) for better justification of the low-temperature polynomial equation of resistivity data. As a result, the new low-temperature polynomial equation of resistivity can be written in the following form

$$\rho = \rho_0 - \rho_{0.5} T^{0.5} + \rho_2 T^2 + \rho_{4.5} T^{4.5} + \rho_5 T^5, \tag{13}$$

where the second term $\rho_{0.5} T^{0.5}$ causes by the e–e Coulombic interaction and the last term $\rho_5 T^5$ contributes to the resistivity due to the e-ph interaction mechanism [44]. The experimental data is well-fitted by the equation (13) below $T < T_{\mathrm{MI}}$ which is shown in the figures 7(a) and (b) for SGSMO-1 and SGSMO-2 compounds respectively. The peak value of resistivity at $H = 10$ kOe is several order higher than that of the magnetic fields higher than 10 kOe for the SGSMO-1 compound and as a result to get a clear view of the isofield resistivity data for various magnetic fields, we multiplied the whole resistivity data with some selected factors as shown in figure 7(a). Similarly, the resistivity minima is not clearly visible for all the isofield resistivity data of the SGSMO-2 compound. Therefore, to emphasize the resistivity minima, the magnified portion along with the polynomial fittings of the resistivity data at the low temperature region are shown in the inset of figure 7(b). The best fitted polynomial parameters are revealed in table 2 for both of the studied systems. After the clear observation in the fitting parameters for both the compounds, we have noticed that $\rho_0 > \rho_{0.5} > \rho_2 > \rho_{4.5} > \rho_5 >$, highly recommended the fact that the grain and domain boundaries play a very important character in the low-temperature conduction mechanism.
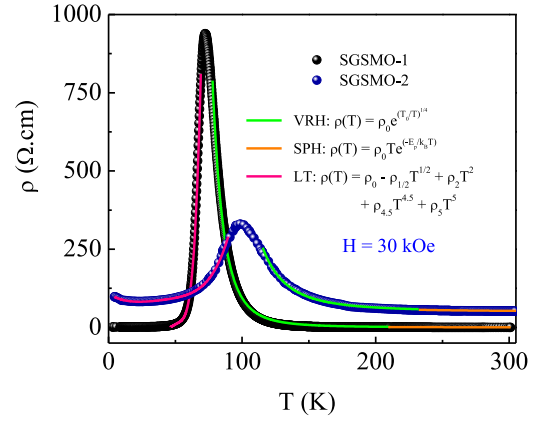

Figure 8. Comparison of electrical resistivity vs T plots along with the fitted lines of different models in the respected temperature regime for SGSMO-1 and SGSMO-2 compounds in presence of 30 kOe magnetic field. The green, orange and pink lines are used to describe the best fitting of the experimental data points in different temperature zones with VRH model, SPH model and low temperature polynomial fit (LT) respectively. The respected fitting equations are also mentioned in the figure.

It is also evident that the values of the fitting parameters progressively decreases with increasing the strength of magnetic fields. The interaction and scattering process between different entities are going to suppress due to the presence of high magnetic field. Among all the mechanisms accounted for the analysis of low-temperature resistivity data, e-e scattering process $(\rho_{0.5})$ is dominated over other interaction/scattering processes. Regarding this context, we must mention that for SGSMO-1 compound, low-temperature resistivity data was tried to fit with equation (12), whereas the best fitting is obtained by using equation (13).

The observed variation of electrical resistivity with temperature along with the different conduction models are briefly visualized in figure 8 for both the compounds SGSMO-1 and SGSMO-2 under the application of $H = 30$ kOe magnetic field. The whole temperature range of the resistivity data is well-explained by SPH model, VRH model and low-temperature polynomial equation (equation (13)) generated due to the presence of various interactions and scattering mechanisms. The SPH model is successfully applied up to the half of the Debye temperature $(\theta_D/2)$ from room temperature in case of both the compounds. In between T_{MI} and $\theta_D/2$, VRH model is found suitable to explain the conduction mechanism. Below T_{MI}, the FM-metallic part is well-understood with the help of temperature dependence of polynomial fitting of residual resistivity, e–e scattering process, magnon spin wave scattering process, e–e Coulombic interaction and e–ph interaction mechanism.

4. Conclusions

To conclude, we have carried out detailed studies on the electrical transport properties of $(Sm_{0.7}Gd_{0.3})_{0.55}Sr_{0.45}MnO_3$ (glassy magnetic ground state) and $(Sm_{0.5}Gd_{0.5})_{0.55}Sr_{0.45}MnO_3$ (ferromagnetic ground state) compounds both in presence and

absence of external magnetic fields. The experimental outcomes exhibit that the transport properties in both the systems are markedly influenced by their respective ground states. In addition to that, we have addressed the low field MR part by considering the spin polarized transport mechanism. At high temperature (paramagnetic–insulator) region, electronic transport mechanism is analyzed by using different suitable models viz SPH and VRH models. Moreover, our study indicates that the upturn in the low temperature electrical resistivity data is well governed by the several types of interaction mechanisms.

Conflict of interest

The authors declare that they have no known competing financial interests or personal relationships that could have appeared to influence the work reported in this paper.

Acknowledgments

Data availability statement

The data that support the findings of this study are available upon reasonable request from the authors.

ORCID iDs

Dipak Mazumdar ![ORCID] https://orcid.org/0000-0001-7975-2819
Kalipada Das ![ORCID] https://orcid.org/0000-0001-7895-518X

References

[1] Tokura Y 2000 *Colossal Magnetoresistive Oxides* (London: Gordon and Breach)
[2] Rao C N R and Raveau R 1998 *Colossal Magnetoresistance, Charge Ordering and Related Properties of Manganese Oxides* (Singapore: World Scientific)
[3] Uehara M, Mori S, Chen C H and Cheong S-W 1999 *Nature* **399** 560
[4] Baldini M, Muramatsu T, Sherafati M, Mao H-k, Malavasi L, Postorino P, Satpathy S and Struzhkin V V 2015 *Proc. Natl Acad. Sci. USA* **112** 10869
[5] Arulraj A, Santhosh P N, Gopalan R S, Guha A, Raychaudhuri A K, Kumar N and Rao C N R 1998 *J. Phys.: Condens. Matter* **10** 8497
[6] Tokura Y and Tomioka Y 1999 *J. Magn. Magn. Mater.* **200** 1
[7] Das K, Dasgupta P, Poddar A and Das I 2016 *Sci. Rep.* **6** 20351
[8] Banik S, Das K, Paramanik T, Lalla N P, Satpati B, Pradhan K and Das I 2018 *NPG Asia Mater.* **10** 923
[9] Biswas A, Chandra S, Phan M-H and Srikanth H 2012 *J. Alloys Compd.* **545** 157
[10] Biswas A, Samanta T, Banerjee S and Das I 2008 *Appl. Phys. Lett.* **92** 212502
[11] Das K and Das I 2015 *J. Appl. Phys.* **117** 175103
[12] Tokura Y 2006 *Rep. Prog. Phys.* **69** 797
[13] Jin S, Tiefel T H, McCormack M, Fastnacht R A, Ramesh R and Chen L H 1994 *Science* **264** 413
[14] Das K, Rawat R, Satpati B and Das I 2013 *Appl. Phys. Lett.* **103** 202406
[15] Kasai M, Kuwahara H, Tomioka Y and Tokura Y 1996 *J. Appl. Phys.* **80** 6894
[16] Chand U, Yadav K, Gaura A and Varma G D 2010 *Optoelectron. Adv. Mater. Rapid Commun.* **4** 11
[17] Culo M, Basletic M, Tafra E, Hamzic A, Tomic S, Fischgrabe F, Moshnyaga V and Korin-Hamzic B 2017 *Thin Solid Films* **631** 205
[18] Mazumdar D, Das K and Das I 2020 *J. Magn. Magn. Mater.* **502** 166507
[19] Mazumdar D, Das K and Das I 2021 *J. Magn. Magn. Mater.* **519** 167413
[20] Nagaraja B S, Rao A, Babu P D and Okram G S 2015 *Physica B* **479** 10
[21] Imada M, Fujimori A and Tokura Y 1998 *Rev. Mod. Phys.* **70** 1039
[22] Martin C, Maignan A, Hervieu M and Raveau B 1999 *Phys. Rev. B* **60** 12191
[23] Tomioka Y, Hiraka H, Endoh Y and Tokura Y 2006 *Phys. Rev. B* **74** 104420
[24] Egilmez M, Chow K H, Jung J, Fan I, Mansour A I and Salman Z 2008 *Appl. Phys. Lett.* **92** 132505
[25] Saitoh E, Tomioka Y, Kimura T and Tokura Y 2000 *J. Phys. Soc. Japan* **69** 2403
[26] Giri S K and Nath T K 2014 *J. Appl. Phys.* **115** 05392
[27] Garcia-Landa B, De Teresa J M, Ibarra M R, Ritter C, Drost R and Lees M R 1998 *J. Appl. Phys.* **83** 15
[28] Sagar S and Anantharaman M R 2012 *Bull. Mater. Sci.* **35** 41
[29] Tomioka Y, Okimoto Y, Jung J H, Kumai R and Tokura Y 2003 *Phys. Rev. B* **68** 094417
[30] Phan M-H and Yu S-C 2007 *J. Magn. Magn. Mater.* **308** 325
[31] Rawat R, Chaddah P, Bag P, Das K and Das I 2012 *J. Phys.: Condens. Matter* **24** 416001
[32] Bukhanko F N 2012 *Phys. Res. Int.* **2012** 1
[33] Raychaudhuri P, Nath T K, Nigam A K and Pinto R 1998 *J. Appl. Phys.* **84** 2048
[34] Raychaudhuri P, Sheshadri K, Taneja P, Bandyopadhyay S, Ayyub P, Nigam A K, Pinto R, Chaudhary S and Roy S B 1999 *Phys. Rev. B* **59** 13919
[35] Dey S and Dey T K 2006 *Bull. Mater. Sci.* **29** 633
[36] Dey P and Nath T K 2006 *Phys. Rev. B* **73** 214425
[37] Banik S, Banu N and Das I 2018 *J. Alloys Compd.* **745** 753
[38] Banik S, Das K and Das I 2019 *J. Magn. Magn. Mater.* **490** 165443
[39] Wagner P, Gordon I, Trappeniers L, Vanacken J, Herlach F, Moshchalkov V V and Bruynseraede Y 1998 *Phys. Rev. Lett.* **81** 3980
[40] Hundley M F, Hawley M, Heffner R H, Jia Q X, Neumeier J J, Tesmer J, Thompson J D and Wu X D 1995 *Appl. Phys. Lett.* **67** 860
[41] O'Donnell J, Onellion M, Rzchowski M S, Eckstein J N and Bozovic I 1996 *Phys. Rev. B* **54** R6841
[42] Xiong G C, Bhagat S M, Li Q, Domínguez M, Ju H L, Greene R L, Venkatesan T, Byers J M and Rubinstein M 1996 *Solid State Commun.* **97** 599
[43] Kusters R M, Singleton J, Keen D A, McGreevy R and Hayes W 1989 *Physica B* **155** 362
[44] Amara G M, Dhahri A, Dhahri J and Hlil E K 2017 *RSC Adv.* **7** 10928
[45] Khan W, Naqvi A H, Gupta M, Husain S and Kumar R 2011 *J. Chem. Phys.* **135** 054501
[46] Modi A, Bhat M A, Pandey D K, Tarachand S, Bhattacharya S, Gaur N K and Okram G S 2017 *J. Magn. Magn. Mater.* **424** 459

[47] Vadnala S, Asthana S, Pal P and Srinath S 2013 *ISRN Mater. Sci.* **2013** 728195

[48] Kurian J and Singh R 2011 *J. Alloys Compd.* **509** 5127

[49] Banerjee A, Pal S and Chaudhuri B K 2001 *J. Chem. Phys.* **115** 3

[50] Ren S, Ma C, Cheng S, Lu L, Shen L and Liu M 2018 *Thin Solid Films* **660** 399

[51] Jung W H 1998 *J. Mater. Sci. Lett.* **17** 1317

[52] Zener C 1951 *Phys. Rev.* **81** 440–4

[53] Hcini S, Khadhraoui S, Zemni S, Triki A, Rahmouni H, Boudard M and Oumezzine M 2013 *J. Supercond. Nov. Magn.* **26** 2181

[54] Viret M, Ranno L and Coey J M D 1997 *Phys. Rev.* B **55** 8067

[55] Synder G J, Hiskes R, DiCarolis S, Beasley M R and Geballe T H 1996 *Phys. Rev.* B **53** 14434

[56] Rana D S, Markna J H, Parmar R N, Kuberkar D G, Raychaudhuri P, John J and Malik S K 2005 *Phys. Rev.* B **71** 212404